RSC Advances

PAPER

View Article Online
View Journal | View Issue

Cite this: *RSC Adv.*, 2026, **16**, 17997

Sodium alginate–poly(vinyl pyrrolidone) pH-responsive hydrogels for controlled release of tinidazole

Zerihun Feyissa Jebessa, *[a] Tariku Bayisa Bedasa,[b] Gemechu Deressa Edossa,[c] Leta Guta Inki,[d] Guta Amenu Abdi[c] and Burka Ahmed Woya[c]

Unlike conventional single polymer hydrogels, cross-linked sodium alginate/poly(vinyl pyrrolidone) provides greater structural integrity and pH-responsiveness. This synergy minimizes premature drug leakage in the upper gastrointestinal tract to ensure targeted drug release specifically to the colon. In this study, sodium alginate–poly(vinyl pyrrolidone) hydrogels were synthesized *via* an ionotropic method, by varying the polymer and $CaCl_2$ concentrations for colon specific controlled release of tinidazole. The hydrogels were characterized using Fourier transform infrared, field emission scanning electron microscopy, X-ray diffraction and thermogravimetric analysis to analyze the structural properties, surface morphology, crystalline structure and thermal stability. Based on swelling and porosity experiments, a 3 : 1 : 3% (w/v) proportion of sodium alginate/poly(vinylpyrrolidone)/$CaCl_2$ was determined as the optimal hydrogel composition for the *in situ* loading of 250 mg of tinidazole. The hydrogels exhibited good *in vitro* biodegradability and improved mechanical strength. The drug loaded hydrogel showed lower cumulative tinidazole release in acidic conditions (pH 1.2) in comparison to the drug release in simulated body fluid (pH 7.4), suggesting the stability of the hydrogels in the hostile environment of the stomach. Kinetic modeling indicated that the release profile was best fit with the Korsmeyer–Peppas model following swelling and diffusion controlled anomalous mechanism. The drug loaded hydrogel has shown strong antibacterial activity against *B. fragilis*. Thus, sodium alginate–poly(vinyl pyrrolidone) hydrogels have promising application for colon specific oral controlled release of tinidazole.

Received 22nd January 2026
Accepted 30th March 2026

DOI: 10.1039/d6ra00524a

rsc.li/rsc-advances

1. Introduction

Hydrogels, which are polymeric materials having three-dimensional cross-linking structures, have attracted attention for oral controlled drug release systems (CDRSs) due to their ease of preparation and easily tunable physicochemical features.[1] A further key characteristic of hydrogels is their ability to show detectable size changes in response to surrounding triggers (*e.g.*, pH, temperature, and ionic strength) without dissolving.[2] The pH-responsive hydrogels commonly contain functional groups such as carboxylate (COO^-), hydroxyl (–OH), and amino ($–NH_2$) groups that can be protonated or deprotonated in various physiological fluids. When the pH of the surrounding medium is higher than the pK_a of the functional group, it is deprotonated; when the pH of the surrounding media is lower than pK_a, it is protonated, resulting in a change in the hydrophilicity of the hydrogel.[3] Because of these amazing properties, pH-sensitive hydrogels exhibit swelling and biodegradability in various media, making them suitable for oral CDRSs.

Hydrogels can be produced *via* physical or chemical gelation methods from a variety of biocompatible, biodegradable, and non-toxic natural polymers comprising alginate, chitosan, silk, gelatin, cellulose, and xanthan gum, and synthetic polymers including poly(vinylpyrrolidone), poly(acrylic acid), poly(ethylene glycol), poly(hydroxyethyl methacrylate).[4] Sodium alginate (SA) and polyvinylpyrrolidone (PVP) have been employed in drug delivery applications owing to their non-toxicity, mucoadhesive nature, and biodegradability. SA is produced by the alkaline treatment of brown algae, is the most versatile, hydrophilic, and biocompatible natural polymer.[5] SA has a linear structure consisting of varying composition of β(1–4)-connected β-mannuronic acid (M) and α(1–4)-connected L-guluronic acid (G) and with carboxylic (COO^-) and hydroxyl (–OH) functional ends.[6] PVP is a hydrophilic, biocompatible,

[a]*Department of Chemistry, College of Natural and Computational Sciences, Bule Hora University, P. O. Box 144, Bule Hora, Ethiopia. E-mail: zerihun.feyissa@bhu.edu.et; Tel: +251 21761050*

[b]*Department of Chemistry, College of Natural and Computational Sciences, Wollega University, P. O. Box 395, Nekemte, Ethiopia. E-mail: tariku.bayisa@astu.edu.et*

[c]*Department of Applied Chemistry, School of Applied Natural Science, Adama Science and Technology University, P. O. Box 1888, Adama, Ethiopia. E-mail: guta.amenu@astu.edu.et; burka.ahmed@astu.edu.et*

[d]*Department of Applied Biology, School of Applied Natural Science, Adama Science and Technology University, P. O. Box 1888, Adama, Ethiopia. E-mail: leta.guta@astu.edu.et*

biodegradable, non-toxic, temperature and pH stable synthetic polymer.[7] PVP has ring-shaped structure which allows controlling porosity and inhibits crystal formation in crosslinked hydrogel systems, making it a convenient polymer for managing drug release patterns.[8]

In their pristine state, SA chains exhibit poor mechanical strength and fragile structures in physiological fluids and degrade after swelling leading to rapid drug release, within a few hours.[9] Similarly, PVP alone exhibits weak mechanical characteristics and swelling properties. Furthermore, failure of the CDRSs design due to inappropriate polymer ratio and crosslinker concentrations may result in slow stimuli responsiveness of hydrogels, difficulty in dosage adjustment, swiftly burst drug release, and poor drug bioavailability.[10] All of these factors may reduce the amount of drug required to enter the lower gastrointestinal tract (colon) for the intended specific therapeutic effect. By crosslinking PVP with SA structures, features including controllable porosity and improved mechanical strength can be obtained, which is required for CDRSs in the colon.

The colon has the greatest microorganism population of any human-related microbes, with the major species being anaerobic bacteria.[11] Because of this, the colon is commonly affected by a variety of persistent inflammatory disorders such as ulcerative colitis, Crohn's disease, and a condition known as irritable bowel syndrome.[12] Tinidazole (TNZ) is an essential orally administered drug for the treatment of colon infections globally due to its renowned reliability and efficacy in clinical applications.[6,13] Colon specific oral CDRSs require less drug release in the upper gastrointestinal tract, allowing the drug to enter the colon at optimal concentration for the desired therapeutic effect. Furthermore, the CDRSs maintain the efficacy of the prescribed therapeutic dosage over an extended period of time while minimizing adverse side effects and enhancing patient safety.[14] SA/PVP hydrogels are increasingly required for CDRSs in the colon, as they are stable in acidic medium (gastric), minimizing drug release in the stomach and helps the drug to reach the colon at optimal therapeutic level.

SA/PVP hydrogels may contribute to antimicrobial activity through several mechanisms. They are known to respond to environmental stimuli (*e.g.*, pH) and undergo swelling. When these hydrogels are loaded with various antibiotics such as TNZ, they can release the drugs in a controlled and sustained manner over time, enhancing antimicrobial activity. By modulating the pH of the environment, they can inhibit the growth of certain bacteria, enhancing the antimicrobial effect. Furthermore, the high water content and hydrophilicity of the hydrogel can disrupt bacterial cell membranes and inhibit microbial growth.

Some previous investigations have reported on CDRSs that use SA and PVP blends or inter-penetrating polymer networks (IPN) materials. SA/PVP hydrogels for controlled release application of paracetamol was reported.[15] A pH-responsive SA/PVP/gelatin hydrogel blends were developed for an *in vitro* controlled release study of nifedipine.[16] Rajeev *et al.*[17] reported SA/PVP loaded with lapatinib for oral drug delivery applications.

While the previous literature has explored the basic biocompatibility of SA/PVP blends, there remains necessity for hydrogels that withstand the harsh gastric environment maintaining sustained drug release in the colon. Unlike prior reports that focused on simple binary blends, this work introduces a double cross-crosslinked SA/PVP hydrogel design to address the limitations of rapid drug leaching, providing colon targeted drug release applications. Moreover, to our knowledge, no research on crosslinked SA/PVP hydrogels loaded with TNZ for colon-specific controlled release and antibacterial efficacy has been published.

In this study, we report crosslinked SA/PVP pH-responsive hydrogels using $CaCl_2$ as crosslinking agent. The polymers ratio and the crosslinker concentration effects on the hydrogel properties were studied to select the optimum composition for drug loading. TNZ were loaded to the hydrogels by *in situ* gelation method. The chemical and surface properties of the hydrogels were characterized using FTIR, FESEM, XRD, TGA, as well as swelling and *in vitro* biodegradation studies. Drug release behavior of the hydrogel was investigated in different pH media. The antimicrobial activity tests were determined for the TNZ loaded hydrogel against *Bacteroides fragilis* and *Pseudomonas aeruginosa* bacteria.

2. Materials and methods

2.1. Materials

PVP-30, having molecular mass of 40 000 g mol^{-1}, food grade SA (91%), analytical grade hydrochloric acid (37.5%), calcium chloride (98%), sodium hydroxide (99%), and absolute ethanol (97.6%) was all acquired from Sisco Research Laboratory Pvt. Ltd in India. Di-basic sodium phosphate (99%), sodium chloride (99%), monobasic potassium phosphate (99%), potassium chloride (99%), and Mueller Hinton Agar (MHA, Oxoid CM0337) were all procured from Sigma-Aldrich Corp. (USA). Addis Pharmaceuticals Factory S.C. (Ethiopia) provided pristine TNZ drug. *B. fragilis* (ATCC 25285), *P. aeruginosa* (ATCC 27853), and Tryptone Soy broth (BK046, UK) were provided by Adama Public Health Research and Referral Laboratory Center. All the chemical reagents were biological grade and utilized as obtained, with double distilled water.

2.2. Synthesis of SA/PVP hydrogels and TNZ loading

SA/PVP hydrogels were synthesized according to previous study using an ionotropic gelation method.[18] SA and PVP clear solutions were separately prepared by dissolving the required polymers proportion (Table 1) in 150 mL of double distilled water. The clear PVP solution was gradually added to the SA solution

Table 1 Proportion of SA/PVP hydrogels

Samples	SA : PVP weight proportion (total weight 6 g)	Calcium chloride solution
S1	3 : 1	3%
S2	1 : 1	3%
S3	1 : 3	3%
S1P1	3 : 1	1%
S1P2	3 : 1	5%

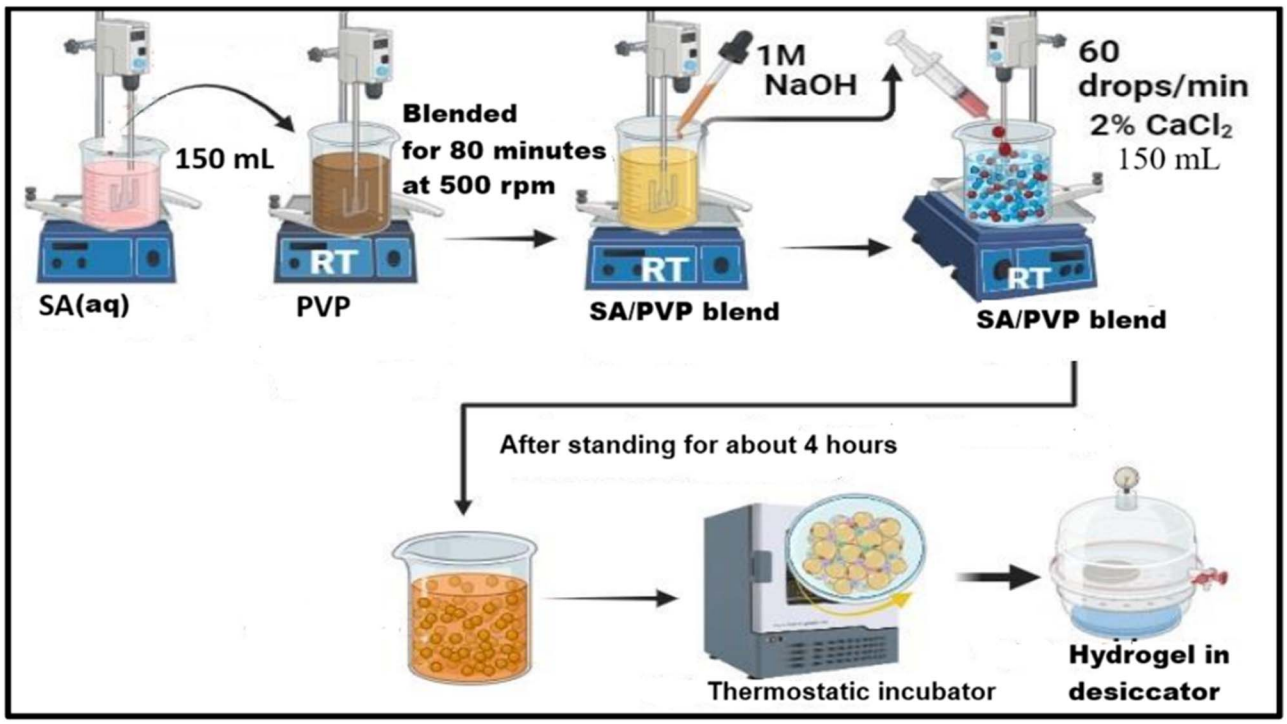

Fig. 1 Schematic of the experimental setup for SA/PVP hydrogel preparation.

and stirred at 500 rpm for 80 minutes at ambient temperature using motor stirrer. The pH of the SA/PVP mixture was attuned to about 5.0 using NaOH aqueous solution (1.0 M) while string. The polymer working mass was then transferred to a beaker containing 150 mL aqueous solution of 2% $CaCl_2$ drop-wise (60 drops per minute) using a syringe while string at 500 rpm. After standing for about 4 hours, the reaction mass was rinsed with double distilled water and filtered using Whatman filter paper (Grade 42). The resulting mass was transferred to glass Petri dishes and placed in a thermostatic incubator for drying at 40 °C for 24 hours, then stored in a desiccator for preservation and further study. A schematic representation of the SA/PVP hydrogels preparation is shown in Fig. 1.

For TNZ loading, 250 mg of TNZ was loaded into an optimal hydrogel (S1) prepared following the same procedure described above. The drug was dissolved in 150 mL double distilled water and slowly added to SA solution while stringing. Following that, SA solution containing the drug and PVP were mixed and stirred at 500 rpm for about 80 minutes at the ambient temperature. Then, the same procedure stated for the synthesis of SA/PVP hydrogels was followed. The hydrogel was coded as TNZ–S1.

2.3. Characterization

2.3.1. Fourier transform infrared spectroscopy. Fourier transform infrared spectrometer (Alpha T, Bruker, Germany) was used to obtain FTIR spectra of the pure polymers (PVP and SA), the drug (TNZ), and the synthesized hydrogels. The powdered dry hydrogel samples were uniformly mixed with KBr powder and pressed into pellets. The FTIR spectra of the pellets were recorded in the wavelength range of 4000–400 cm^{-1} with resolution of 4 cm^{-1} at a scanning rate of 80 scans per minute.

2.3.2. X-ray diffraction analysis. XRD analysis was done for the hydrogels as function of concentrations of crosslinking agent and drug loading on the phase nature of the hydrogels employing XRD instrument (XRD 7000, SHIMADZU, Japan). The XRD data were taken by using CuKα (1.5406 Å) radiation source, in 2θ range of 5°–60° at a scanning rate of 0.02 s^{-1}, 40 kV applied voltage and current of 30 mA at room temperature.

2.3.3. Thermogravimetric analysis. The thermal stability of the pure polymers (PVP and SA), the pure TNZ, and the hydrogels was investigated using thermal analyzer instrument (BJ HENVEN, China), in a temperature range of 25–700 °C under gas flow rate of 20 mL min^{-1} and at heating rate of 10 °C min^{-1}.

2.3.4. Scanning electron microscopy. The surface morphologies of the hydrogels (S1, S1P1, S1P2, and TNZ–S1) were acquired using field emission scanning electron microscopy (Apreo, Thermo Fisher Sci., Singapore) with regard to the pore distribution and incorporation of the drug using. The hydrogels were coated with a tiny layer of gold particles using sputtering method before imaging.

2.3.5. Mechanical properties. The tensile strength (TS) and elongation at break (EB%) were determined for the synthesized SA/PVP hydrogels. A tensile strength testing machine (Instron, model 3400, UK) was used. The hydrated hydrogel samples were cut into dumbbell-shape strip (50 mm × 10 mm). The tests were performed using a load cell of 100 N at ambient temperature with a speed of 10 mm min^{-1}. Each test was repeated five times and the average TS and EB (%) were calculated using equations previously described.[19]

2.3.6. Biodegradation analysis. SA/PVP hydrogels crosslinked with varying concentrations of $CaCl_2$ (1%, 3%, and 5%) and the drug loaded hydrogel (TNZ–S1) were submerged in the

body fluid (pH 7.4) and incubated at 37.2 °C while shaking at 100 rpm for fourteen days (14) days. The hydrogels were weighed (W_0) after completely swelled. The *in vitro* biodegradation was measured gravimetrically at specified time interval of 1, 3, 5, 7, 9, 11, 13, and 14 days by taking out the hydrogels from the fluids, cleaned properly with filter paper, and weighed (W_f). Fresh SBF was used to maintain the volume of the fluid.[20] Weight loss (%) was determined using eqn (1):

$$\text{Weight loss (\%)} = (W_f - W_0)/W_0 \times 100 \quad (1)$$

2.3.7. Swelling property. The swelling ratio (SR) of the hydrogels were evaluated by submerging a known weight (W_0) triplicates of hydrogel samples in 50 mL of SGF (pH 1.2), SIF (pH 6.5), and SBF (pH 7.4), which were prepared following a previously outlined procedure[21] and maintained at 37.2 °C under shaking at 80 rpm. At predetermined interval of time: 30, 60, 90, 120, 150, 180, 210, and 240, 270, 300, and 360 minutes, the hydrogels were taken out of the simulated fluids, carefully cleaned by filter papers, and weighed (W_f). SR (%) was calculated using eqn (2):

$$\text{SR (\%)} = (W_f - W_0)/W_0 \times 100 \quad (2)$$

2.3.8. Porosity measurement. Porosity of the synthesized hydrogel samples was measured using a solvent replacement process.[22] 25 mL of absolute ethanol as an inert solvent and preweighed hydrogel sample (W_H) were added to a beaker of known weight (W_0), and the total weight was obtained (W_1). The hydrogel samples were taken out after 24 hours and the parts left over were weighed (W_2). The porosity (%) of the hydrogels was determined using eqn (3), where ρ_e represents the density of the ethanol (g mL^{-1}).

$$\text{Porosity (\%)} = (W_1 - W_2 - W_H)/(W_0 - W_2 + 25\rho_e) \times 100 \quad (3)$$

2.3.9. Drug release profile. The TNZ–S1 hydrogels were tested for drug release *in vitro* by submerging in 40 mL of SGF, SIF, and SBF and incubated at 37.2 °C in a thermostatic shaking incubator with fixed shaking rate at 80 rpm. At defined time intervals of 1, 2, 3, 4, 5, 6, 7, 8, 9, 10, 11, 12, 13, 14, 15, 24, 28, 32, 36, 40, and 48 hours, 5 mL supernatant of each incubated sample was extracted. Then, the absorbance was obtained using a UV spectrophotometer at a wavelength of 278 nm. The drug concentration was measured using a calibration curve derived from standard solutions of TNZ (0.5, 2, 4, 6, 8, 10, 12 g mL^{-1}) in triplicate. The cumulative drug concentration released by the matrix was computed using eqn (4):

$$\text{Cumulative drug release (\%)} = \frac{50C_t + \sum 5C_{t-1}}{W_0} \times 100 \quad (4)$$

where; W_0 represents the initial amount of a drug incorporated into the hydrogel, and C_t and C_{t-1} represent the concentration of drug released at time t and t_{-1}.

2.3.10. Drug release mechanisms. The *in vitro* drug release kinetics and mechanisms were determined by incorporating the release data into zero order, first order, Higuchi, and Korsmeyer–Peppas mathematical models.

2.3.11. Antibacterial activity test. The antibacterial activity of the TNZ-loaded hydrogel was evaluated following the Kirby–Bauer disk diffusion susceptibility test protocol at Adama Public Health Research and Referral Laboratory Center against *B. fragilis* (ATCC 25285) and *P. aeruginosa* (ATCC 27853). The unloaded hydrogel (S1) and the pristine TNZ were used as negative and positive control, respectively. The inoculum was prepared by transferring 5 colonies of each strain into an appropriate Tryptone Soy broth (BK046, UK) placed in an incubator at 37.2 °C for 6 hours until an opacity was obtained which is equivalent to the standard opacity of a barium sulfate suspension (density of 0.5 on the McFarland scale) measured by McFarland densitometer (DEN-1B). The opacity of the inoculum was adjusted to the standard using a sterilized phosphate buffered saline (PBS) and excess broth was drained by pressing the swab on the walls of the tube. Each bacterial stock of estimated concentration of approximately 1×10^8 cells per mL was obtained.

The antibacterial activity test was done using MHA medium. Sterilized MHA media was poured into sterilized Petri-dishes and solidified. A 100 μL of each bacterial stock with an estimated 1×10^8 cells per mL concentration was uniformly dispersed on the Petri-dish plates containing MHA media. Then, UV sterilized TNZ–S1 hydrogel of appropriate size and 20 μL control samples of TNZ (1 mg mL^{-1}) poured onto a 6 mm-diameter filter paper that had undergone UV sterilization were placed on the agar plates' surface containing bacterial suspension. The dishes were incubated upside down at 37.2 °C. For the *B. fragilis* assays, the dishes were in a 2.5 L jar containing an Oxoid™ AnaeroGen™ 2.5 L sachets for overnight to create anaerobic conditions. In contrast, the testing against *P. aeruginosa* was conducted separately under normal aerobic conditions. The inhibition zone was assessed by determining the diameter of the zone of inhibition in triplicate.

2.3.12. Statistical analysis. Origin 2021b version software was used to analyze statistical data and generate figures. Data is provided as means ± standard deviation (SD) from triplicate experiments.

3. Results and discussion

SA/PVP hydrogels prepared during the preliminary experiment to determine the starting concentration of $CaCl_2$ was highly fragile with 0.5% of $CaCl_2$ due to the SA chains were insufficiently crosslinked. A stable SA/PVP hydrogels was observed with 1% $CaCl_2$ solution.

Fig. 2 demonstrates the proposed formation of the hydrogel network, highlighting the polymer–polymer and polymer–drug crosslinking mechanisms through the combination of chemical and physical interactions. The SA chains are interconnected through an ionic-crosslinking between the bivalent cation (Ca^{2+} ions) and the anionic carbonyl ends of SA (COO^-), resulting in "egg-box" copolymer chains substituting the Na^+ ions.[23]

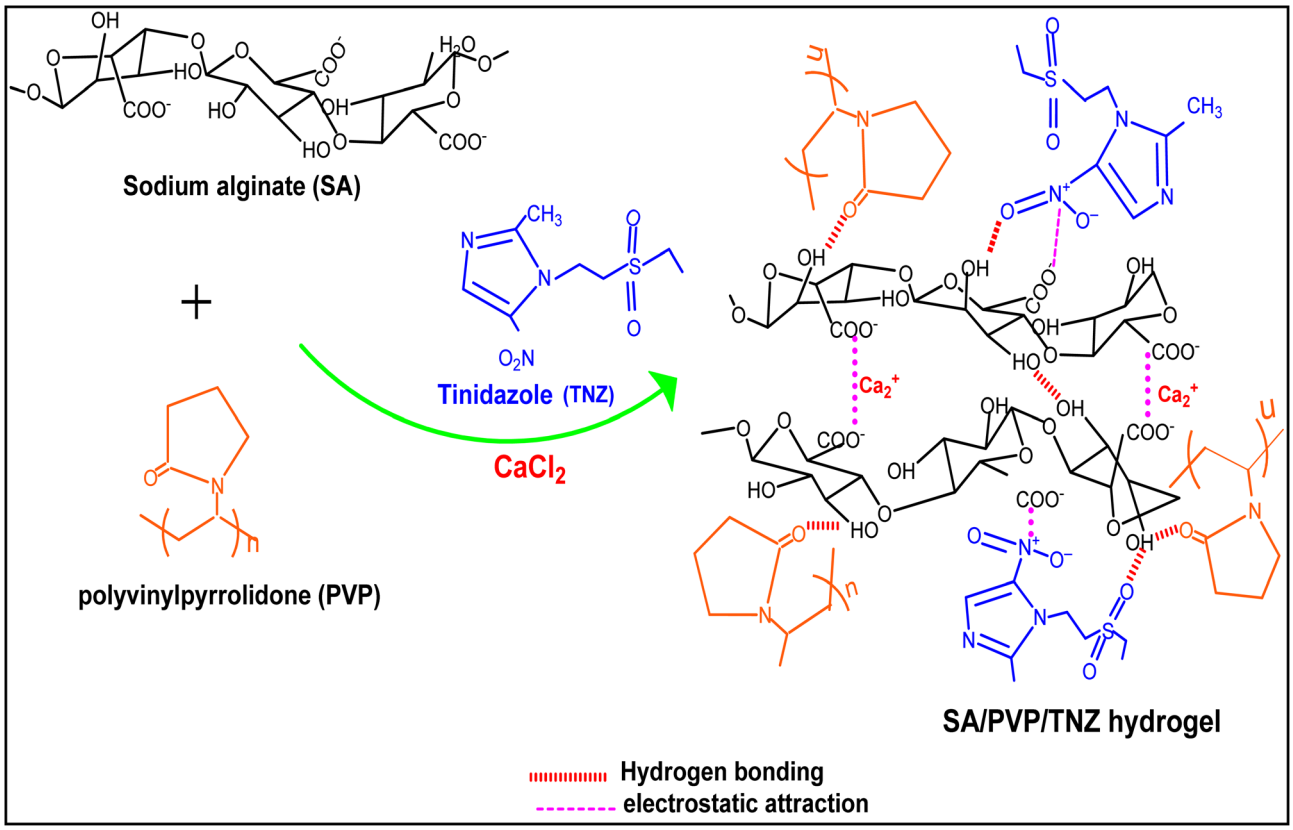

Fig. 2 Schematic diagram showing polymer–polymer and polymer–drug interactions.

Because of the random arrangements of the crosslinked hydrogel networks, the ring-shape PVP chains enter the egg-box networks of SA *via* physical entanglement, forming semi-interpenetrating polymer networks. Likewise, TNZ (hydrophilic) is integrated into the semi-IPNs *via* various intermolecular interactions such as dipole–dipole, electrostatic and hydrogen bonding interactions. During this interactions, the electrons of the nitro groups of TNZ delocalized forming nitroso radicals. FTIR analysis confirmed the expected polymer–polymer and polymer–drug interactions.

3.1. Fourier transform infrared spectra

FTIR (Fourier transform infrared) spectroscopy is an important tool for studying the chemical interactions and structural features of hydrogels used in drug delivery applications. In this study, the FTIR spectra of TNZ-loaded SA/PVP hydrogel can provide insight into drug–polymer interactions, which is critical for understanding how the drug (TNZ) is incorporated into the polymer network. Fig. 3 displays the infrared absorption spectra of PVP, SA, S1, TNZ, and TNZ–S1. PVP exhibits a broad infrared absorption band of O–H bond within a range of 3000–3600 cm^{-1} (Fig. 3a), attributed to the physically absorbed water due to the intrinsic hydrophilic property of PVP.[15] The weak infrared absorption band of PVP observed at 2923 cm^{-1} is associated with the stretching mode of the aliphatic C–H bonds ($-CH_2-$). The strong infrared absorption band at 1656 cm^{-1} caused by the symmetric stretching mode of C=O. The infrared absorption band at 1422 cm^{-1} corresponds to the bending vibration mode of $-CH_2$ group. Other notable bands seen at 1285 cm^{-1} and 1020 cm^{-1} are developed due to stretching mode of C–N–C and C–OH bonds respectively.[15] SA chains (Fig. 3a) showed a broad band of O–H stretching vibration mode ranging between 3000 and 3600 cm^{-1}. The bands at 2920 cm^{-1}, 1595 cm^{-1}, and 1394 cm^{-1}, are caused by the stretching modes of aliphatic C–H bonds ($-CH_2$ group), the symmetric, and asymmetric stretching of carbonyl end (C=O) of carboxylate group (COO^-), respectively. The weak band at 1084 cm^{-1} and the strong band intensity at 1010 cm^{-1} are attributed to C–O and C–O–C stretching modes of SA respectively.[24]

In the hydrogel S1 spectrum (Fig. 3a), the strong infrared absorption band due to –OH stretching mode ranging between 3000 and 3600 cm^{-1} reveals the formation of more hydrogen bonding during the polymer–drug interaction. The weak band at 807 cm^{-1} corresponding to Ca–O stretching mode. The band at 1381 cm^{-1} is due to the bending vibration mode of the $-CH_2-$ group. In the hydrogels, the carbonyl bond (C=O) stretching mode of pristine SA at 1595 cm^{-1} and PVP at 1656 cm^{-1} are shifted to 1650 cm^{-1} with a decreased intensity. The strong band at 1010 cm^{-1} is ascribed to C–O–C of the saccharide structure of SA. These results show the presence of interactions between the anionic alginate carbonyl groups and PVP chains. In the TNZ spectrum (Fig. 3b), the typical stretching vibrational bands at 1520, 1260, 1367, 1300 cm^{-1} assigned to the stretching mode of the imidazole ring (C=N), C=C, nitro (N=O) and

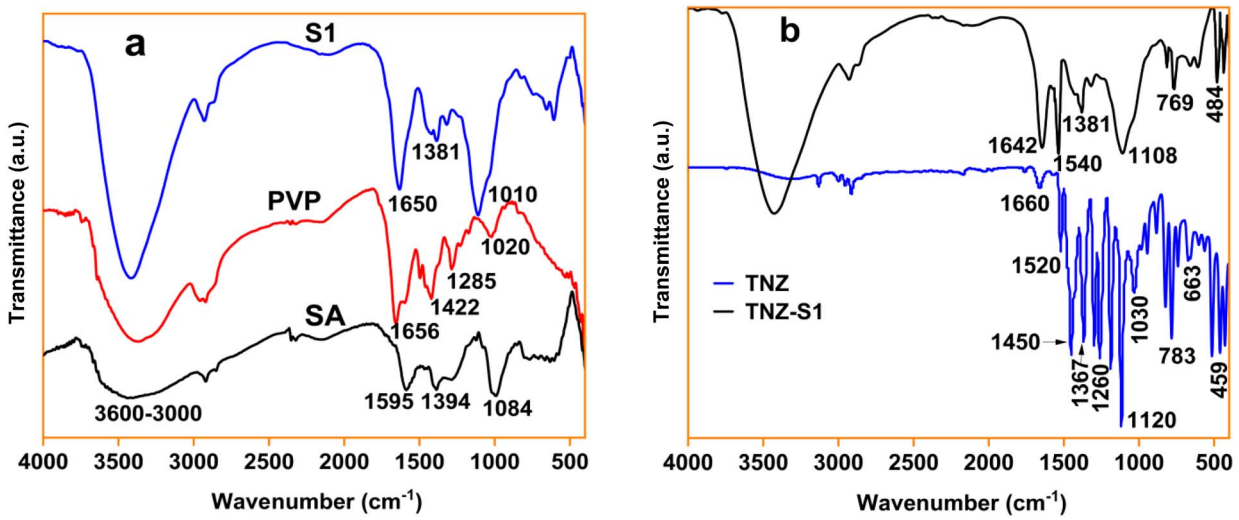

Fig. 3 FTIR spectra of (a) PVP, SA, S1 and (b) TNZ and TNZ–S1.

asymmetric stretching mode of sulfinyl (S═O), respectively.[25] The band at 1450 cm^{-1} is assigned to $-CH_2$ bending vibration mode. Other distinctive infrared absorption bands at 825, 783, 663, and 459 cm^{-1} associated to the deformation and waging vibrational modes of sulphone (O═S═O) group.[26] In the of TNZ–S1 spectrum (Fig. 3b), the characteristic bands at 1642 cm^{-1}, 1260–1030 cm^{-1}, and 1381 cm^{-1} correspond to the C═O, C–O–C of SA saccharide structures, and C–H deformation vibrations, respectively. The absorption band observed at 1540 cm^{-1}, 769 cm^{-1}, and 484 cm^{-1} are associated to the nitro (N–O) bond stretching mode and waging vibrational modes of sulphone (O═S═O) group of TNZ incorporated into the polymer networks.

The FTIR spectra of the hydrogels the shifts in the TNZ-specific bands confirm TNZ's interaction with the polymer matrix, evidenced by peak changes like C═O at 1642 cm^{-1}, C–O–C at 1260 cm^{-1}, and C–H at 1381 cm^{-1}, suggesting interactions with the SA saccharide structure. These changes, particularly around TNZ's functional groups (nitro, sulphone, and imidazole), indicate strong interactions with the polymers (PVP and SA), likely through hydrogen bonding, ionic, or hydrophobic forces. Despite these interactions, TNZ-specific peaks (*e.g.*, 1540 cm^{-1}, 769 cm^{-1}, and 484 cm^{-1}) remain, showing TNZ's functional groups are intact but integrated into the network.[27]

The presence of TNZ-specific peaks in the hydrogel suggests its incorporation into the polymer network, which may enhance the drug release profile and bioactivity. Changes in functional groups and peak shifts suggest tighter drug–polymer interactions, potentially slowing TNZ diffusion for a sustained release. Hydrogen bonding and ionic interactions between SA's carboxylate groups and TNZ's cationic components may improve the drug's stability, contributing to more reliable and controlled release for therapeutic effectiveness.

3.2. X-ray diffraction

Fig. 4 shows the diffractograms of SA, PVP, S1, TNZ, and TNZ–S1. It is observed that PVP shows two broad peaks at 2θ values of approximately 11° and 21°, which are attributed to the reflections emanating from short range arrangements and pseudo-crystalline phase in the noncrystalline structures of PVP respectively.[28] Two major diffraction peaks are observed in the SA diffractogram at 2θ values of approximately 13° and 21°, attributed to the scattering of (110) planes of poly(guluronate) and (200) planes of poly(mannuronate) ends. The diffractograms of the hydrogel S1 and TNZ–S1 show decrease in the intensity of the peaks ranging between 2θ values of 17° and 23° due to the crosslinking agent concentration, enhancing the noncrystalline nature of the hydrogels.

In the crosslinked hydrogels, the hydrogen bonding formed between the carbonyl ends of PVP and the –OH groups of SA, as well as the electrostatic attraction between the divalent cation (Ca^{2+}) and COO^- of SA, promote chain-to-chain secondary bonding, thereby improving crystallinity.

However, at higher concentration of the crosslinker, the hydrogen bonds and electrostatic interactions are disturbed by

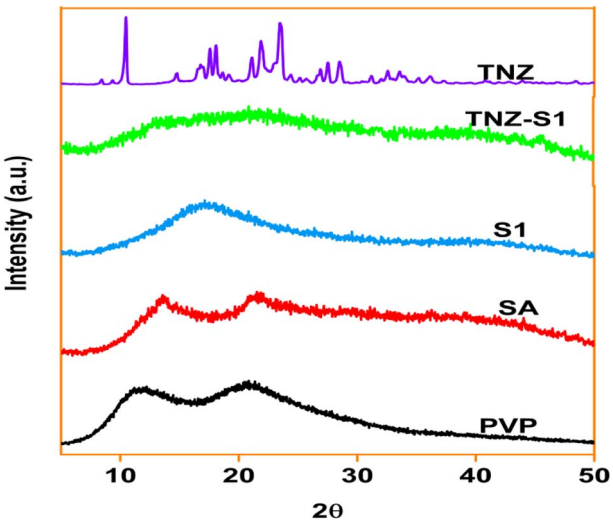

Fig. 4 XRD diffractograms of PVP, SA, S1, TNZ–S1, and TNZ.

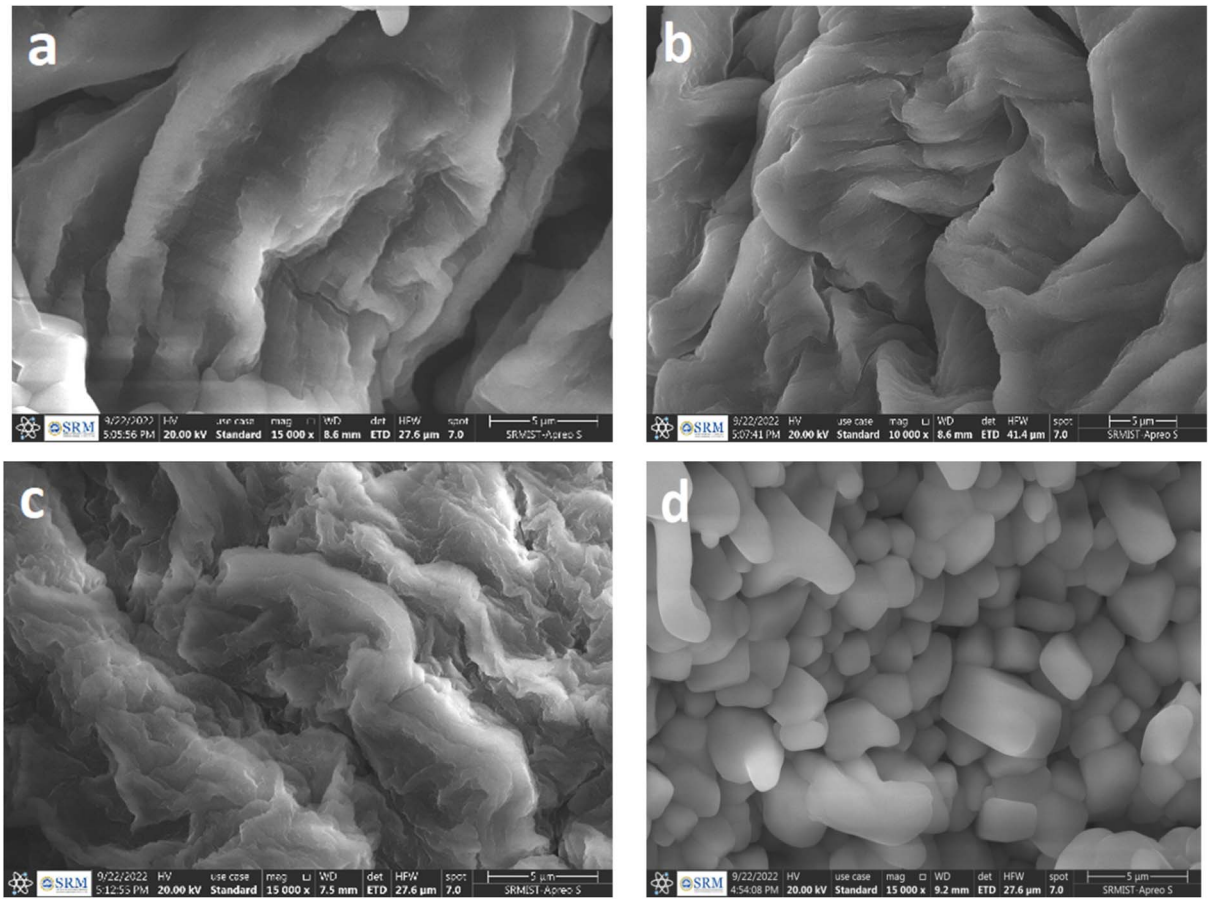

Fig. 5 FESEM micrographs of hydrogel (a) S1, (b) S1P1, (c) S1P2 and (d) TNZ–S1.

increasing crosslinking density, resulting in noncrystalline structures. The diffractogram of TNZ (Fig. 4) exhibited several characteristic peaks at 2θ values of approximately 10.44°, 17.59°, 18.17°, 23.46°, 28.4°, and 32.78° showing its crystalline structure. It is observed that the XRD pattern of the drug loaded hydrogel (TNZ–S1) is similar to the unloaded hydrogels (S1). The sharp peaks detected in the diffractogram of TNZ are repressed, possibly due to the dominance of the noncrystalline nature of the polymers, revealing the incorporation of the drug into the polymer matrix in molecular form.

3.3. Scanning electron microscopy

The surface morphology of the hydrogels as a function of crosslinker ($CaCl_2$) concentration is shown in Fig. 5a–c. The micrographs of S1, S1P1, and S1P2 clearly show the porous and squishy three-dimensional crosslinked structures.

The crosslinker ($CaCl_2$) concentration has a noticeable effect on the size, consistency, and depth of the hydrogel porosity. The sizes of the pore networks decrease as the crosslinker concentration increases from 1% to 5% (S1P1, S1 and S1P2), resulting in a more stiff and denser network structures with smaller pores due to increased crosslinking density. The hydrogel S1P2 had highly compact structures with small pores, which lessen their swelling capacity.

In this work, the pore structure of the hydrogel S1 is considered as an optimal for the controlled-release of the drug (TNZ). Fig. 5d shows the micrograph of the drug loaded hydrogel (TNZ–S1), which is comparatively densely granulated structure, which confirms the successful incorporation of the drug (TNZ) into the hydrogel.

3.4. Thermogravimetric analysis

The thermogravimetric decomposition curves of SA, PVP, S1 and TNZ–S1 are presented in Fig. 6. Pure SA shows three thermal decomposition steps. The initial stage extending approximately up to 200 °C is caused by the loss of both free water (up to 100 °C) and bound water with a degradation rate of approximately 15%. The second stage occurred between temperature zones of 200–340 °C, with thermal decomposition rate of approximately 37%. This is caused by the decomposition of glucosidic bonds in SA chains forming smaller fragment units such as methane (CH_4), water (H_2O), and sodium carbonate (Na_2CO_3).[29]

The last thermal decomposition stage was noted in the temperature zone of 340–650 °C. In this phase, roughly 23% mass is lost due to the entire breakdown of the polymer units, which leads to the emission of gasses (*e.g.*, CO_2) and the formation of ash.[30] The final weight residue of approximately 24.1% was obtained at 650 °C. In the case of PVP three thermal

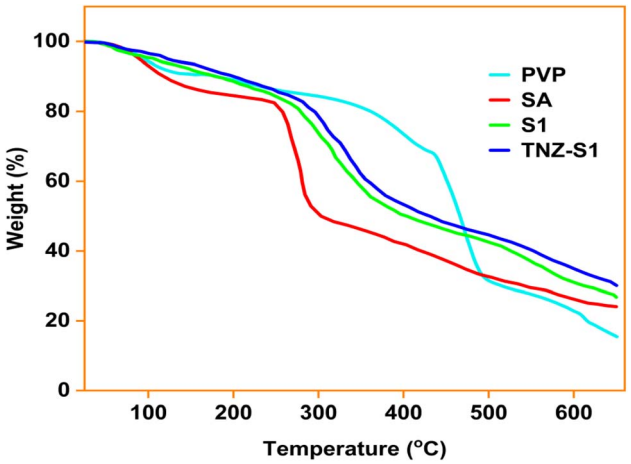

Fig. 6 TGA thermogravimetric curves of PVP, SA, hydrogels S1, and TNZ–S1.

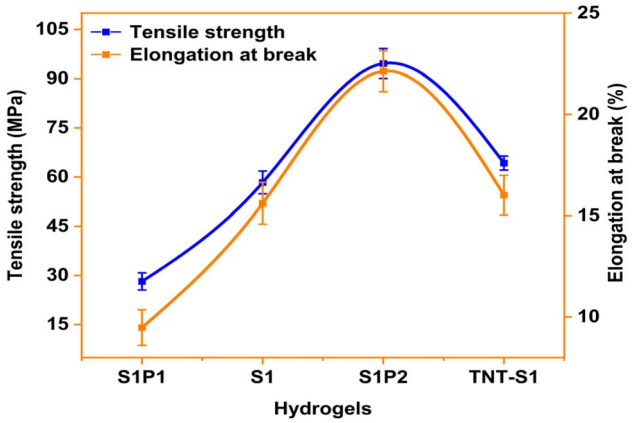

Fig. 7 Mechanical properties of hydrogels S1P1, S1, S1P2, and TNZ–S1.

degradation steps were observed which start in the temperature zone of 25–130 °C ascribed to free water removal. It is followed by a slant ranging from 130 °C to 250 °C with a decomposition rate of approximately 14% attributed to the loss of bound water. The subsequent decomposition stage happened between temperature zones between 250 and 515 °C, with a decomposition rate of approximately 55% induced by partial polymer degradation. The last thermal decomposition stage of PVP was observed between 516 and 650 °C with ash yield of approximately 15% ascribed to the total decomposition of the polymer backbone.

The thermal decomposition behavior of the hydrogels S1 and TNZ–S1 also exhibited three stages with reduced decomposition rate in the initial stage (up to 200 °C) relative to that of pure SA and PVP. This condition is associated with crosslinking effect which decreases the hydrophilic nature of the polymers and, hence water absorption capability of the hydrogels. The major thermal decomposition process was observed in the subsequent step between temperature zones of 200–495 °C. It involves the partial decomposition of hydrogels producing smaller molecules such as acetic acid, butyric acid, smaller fat acids and eventually forming stable aromatic compounds and $CaCO_3$ ash.[31] The last thermal decomposition stage was observed in the temperature zone of 395–650 °C attributed to the complete decomposition of the polymers backbone. The result reveals that crosslinking of the polymers and drug loading improved the hydrogels thermal stability.[32] Overall, the thermal decompositions occur at temperature ranges greater than 37.2 °C, implying that hydrogels are appropriate for CDRSs.

3.5. Mechanical properties

Fig. 7 shows the tensile strength (TS) and elongation at break (EB%) of S1P1, S1, S1P2, and TNZ–S1 hydrogels. The results show that increasing the $CaCl_2$ concentration increased the TS and EB (%) of the hydrogels. The hydrogel S1P1 crosslinked with 1% $CaCl_2$ has a TS of 28.18 ± 2.62 MPa and EB (%) of 8.47 ± 0.88%, whereas the hydrogel S1P2 crosslinked with 5% $CaCl_2$ has TS of 94.61 ± 4.54 MPa and EB (%) of 22.13 ± 1.01%.

The increase in TS and EB (%) with increasing $CaCl_2$ is attributed to the increasing crosslinking density caused by the ionic interactions between the carboxylate groups (COO^-) of SA,[19,33] and Ca^{2+} as well as the physically entangled PVP chains.

The high crosslinking density makes the hydrogel networks highly stiff and improves mechanical properties of both SA and PVP, which helps to overcome rapid dissolution and fast drug, release problem.[34] In this work, the hydrogel S1 with TS of 58.34 ± 3.47 MPa and EB (%) of 15.61 ± 1.03% was selected as a suited for possible applications in sustained colon specific controlled release of TNZ. The drug-loaded hydrogel (TNZ–S1) had TS of 64.25 ± 2.14 MPa and EB (%) of 16.01 ± 0.98. The drug-loaded hydrogel (TNZ–S1) showed significantly improved TS and EB (%) comparing with the unloaded optimal hydrogel (S1) attributed to the enhanced polymer–drug interactions.

3.6. Biodegradation test

The *in vitro* biodegradation profile of the hydrogels S1, S1P1, S1P2, and TNZ–S1 in SBF for 14 days is shown in Fig. 8. The figure shows that the hydrogels exhibited an analogous *in vitro* degradation patterns. Between day 1 and 3, the hydrogels are almost intact, whereas, after 5 days, S1P1, S1, S1P2 and TNZ–S1 degraded at a significantly higher degree with the corresponding weight loss of approximately 28.44 ± 1.86%, 22.58 ± 1.88%, 18.59 ± 1.72%, and 16.75 ± 1.71%, respectively at day 7. It was noticed that mass loss percentage decreases with increasing the crosslinker concentration due to the increasing crosslinking density.[35] At day 14, weight of the hydrogels S1P1, S1, S1P2, TNZ–S1 decreased approximately to 59.09 ± 1.81%, 53.12 ± 1.12%, 43.76 ± 1.9%, and 50.78 ± 1.71%, respectively. The weight loss pattern of TNZ–S1 was observed to be similar to that of S1, except with a reduced rate of degradation, displaying a weight loss of approximately 20.09 ± 1.72% at 7 days.

This could be due to enhanced polymer–drug interactions, resulting in a more tightly crosslinked network structure. SA and PVP are unstable in moist conditions due to their high hydrophilicity and degrade rapidly. SA is deprotonated and less stable in SBF due to an increase in carboxylate groups, increasing the swelling and degradation rate. However,

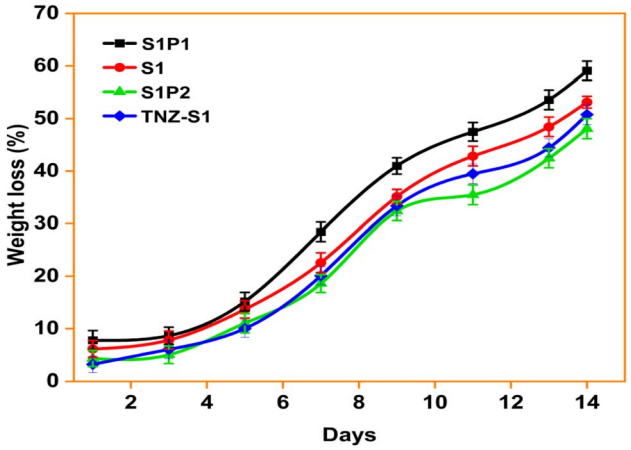

Fig. 8 Biodegradation of hydrogels S1P1, S1, S1P2, and TNZ–S1 in SBF at 37.2 °C.

crosslinking SA and PVP produces a complex 3D network structure, resulting in a more hydrophobic structure.

Increasing $CaCl_2$ concentration further improves the hydrogel's hydrophobicity. This decreases the rate of biodegradation and allows the hydrogels to reach colon for controlled and prolonged release of TNZ by tolerating the impact of the acidic environments of gastric.[36] Despite intensive crosslinking, SA networks yet contain extra carboxylate and hydroxyl groups. The residual non-interacting groups contribute to the hydrolytic decomposition of the cross-linked SA/PVP hydrogels. Furthermore, the Na^+ in the SBF replaces the Ca^{2+} in the egg-box dimer structure, weakening the frameworks and causing the hydrogel to degrade slowly. Because of their slow biodegradability and ease of clearance after a useful lifetime, SA and PVP-based hydrogels developed in this study have a potential in colon specific CDRSs.

3.7. Swelling property

Swelling prosperity is one of the important parameters of crosslinked hydrogels for usage in CDRSs. Fig. 9 shows the SR (%) of the crosslinked hydrogels S1, S2, S3, S1P1 and S1P2 in SGF, SIF, and SBF at 37.2 °C for 360 minutes. As it can be seen from the figure, in acidic medium (SGF), the SR (%) of the SA/PVP hydrogels decrease with increasing SA content and increases with increasing proportion of PVP. The hydrogel S3 (SA/PVP, weight ratio of 1 : 3), displays the maximum SR (%) in SGF in comparison to other SA/PVP hydrogels with maximum values of approximately 275.70 ± 16.07%.

The lowest SR (%) value was observed for hydrogel sample S1 (SA/PVP weight ratio of 3 : 1), with maximum SR (%) values of about 198.23 ± 12.02%, in SGF. This shows that SA is stable in SGF (pH 1.2). In an acidic medium (SGF), the hydrogel S3 had a 37% higher SR (%) than S1 (SA/PVP, weight ratio of 3 : 1) after 360 minutes. The decreased in SR (%) of the hydrogels in SGF as SA content increases is associated with the nature of SA in acidic medium. $CaCl_2$ crosslinks the carboxylate groups (COO^-) of SA through ionic interactions, thereby decreasing the hydrophilic functional groups. However, excess COO^- of SA protonated in acidic medium forming stable algenic acid (–COOH).[37]

Strong hydrogen bonding also occurs between the algenic acid and C=O groups of the polymers, resulting in the development of stiff and denser structures that restrict fluid absorption. The increased in SR (%) of the hydrogels in SGF as PVP content increases is attributed to the increased in porosity and more hydrophilic character of PVP.[38] PVP is interweaved into the SA network through physical interactions and the ring chains of PVP form void spaces inside the semi-IPNs owing to the irregular arrangement of the polymer matrix. As a result, more fluids diffuse into the matrix, occupying the open empty spaces and swelling the hydrogels.

In SIF (pH 6.5) and SBF (pH 7.4), however, the swelling property was inverted in which, SR (%) increased as SA content increased. The hydrogels show the highest swelling ratio in SBF (pH 7.4). As it is observed from Fig. 9 the hydrogel S1 (SA/PVP, 3 : 1) has a swelling ratio of about 401.96 ± 12.1% and 521.94 ± 10.03% in SIF and SBF respectively at 360 minutes. In comparison, hydrogel S3 (SA/PVP, 1 : 3) had the lowest SR (%) of about 291.70 ± 11.95% and 351.53 ± 13.7% in SIF and SBF, respectively. At 360 minutes, the swelling ratio of hydrogel S1 was about 59.88% higher in SBF than in SIF. The observed swelling property of SA/PVP is attributed to the nature of SA in slightly alkaline media. The number of carboxylate ions (COO^-) produced from the deprotonation of the –COOH groups of SA in a slightly alkaline media is higher. Strong electrostatic repulsion forces between the carboxylate ions drive polymer chain expansion, resulting in the uptake of additional fluids which is also attributed to the porous entangled PVP chains.

In SBF (pH 7.4) in comparison to the SIF (pH 6.5) the hydrogels S1 to S3 displayed similar pattern of SR (%), except with slightly higher fluid up take in SBF. The difference in the SR (%) in each fluid indicates the pH-sensitivity of the SA/PVP hydrogels, which is owing to the protonation and deprotonation capability of the carboxylate groups of SA, and the porous hydrophilic PVP ring structure. As mentioned above, pH-sensitive hydrogels for oral colon-specific CDRSs must possess minimal swelling and drug release properties in the acidic medium (stomach) but optimal swelling as well as drug release in the colon tract, where drug activity is the highest.[39] Therefore, in this study the hydrogel S1 (SA/PVP, 3 : 1) is selected as the optimal polymer proportion for TNZ loading, as it indicates a relatively lower swelling ratio in the SGF (pH 1.2) and a relatively higher swelling ratio in the SBF (pH 7.4).

Fig. 9 also shows the SR (%) of the hydrogels as a function of crosslinker concentration (S1, S1P1 and S1P2). In each simulated fluid, the SR (%) decreases with rising $CaCl_2$ content. For instance, the hydrogel S1P1 ($CaCl_2$, 1%) had a SR (%) of about 163.23 ± 8.23%, 182.23 ± 8.1%, and 287.96 ± 18.12% in SGF, SIF and SBF, respectively at 360 minutes. In comparison, hydrogel S1P2 ($CaCl_2$, 5%) had the lowest SR (%) of about 127.45 ± 5.2%, 135.88 ± 6.67%, and 235.68 ± 14.3% in SGF, SIF and SBF, respectively. The increase in SR (%) with rising $CaCl_2$ content is associated with more ionotropic crosslinking of the COO^- groups of SA and the divalent cation (Ca^{2+}), resulting in dense structures that reduce the diffusion of the fluids into the

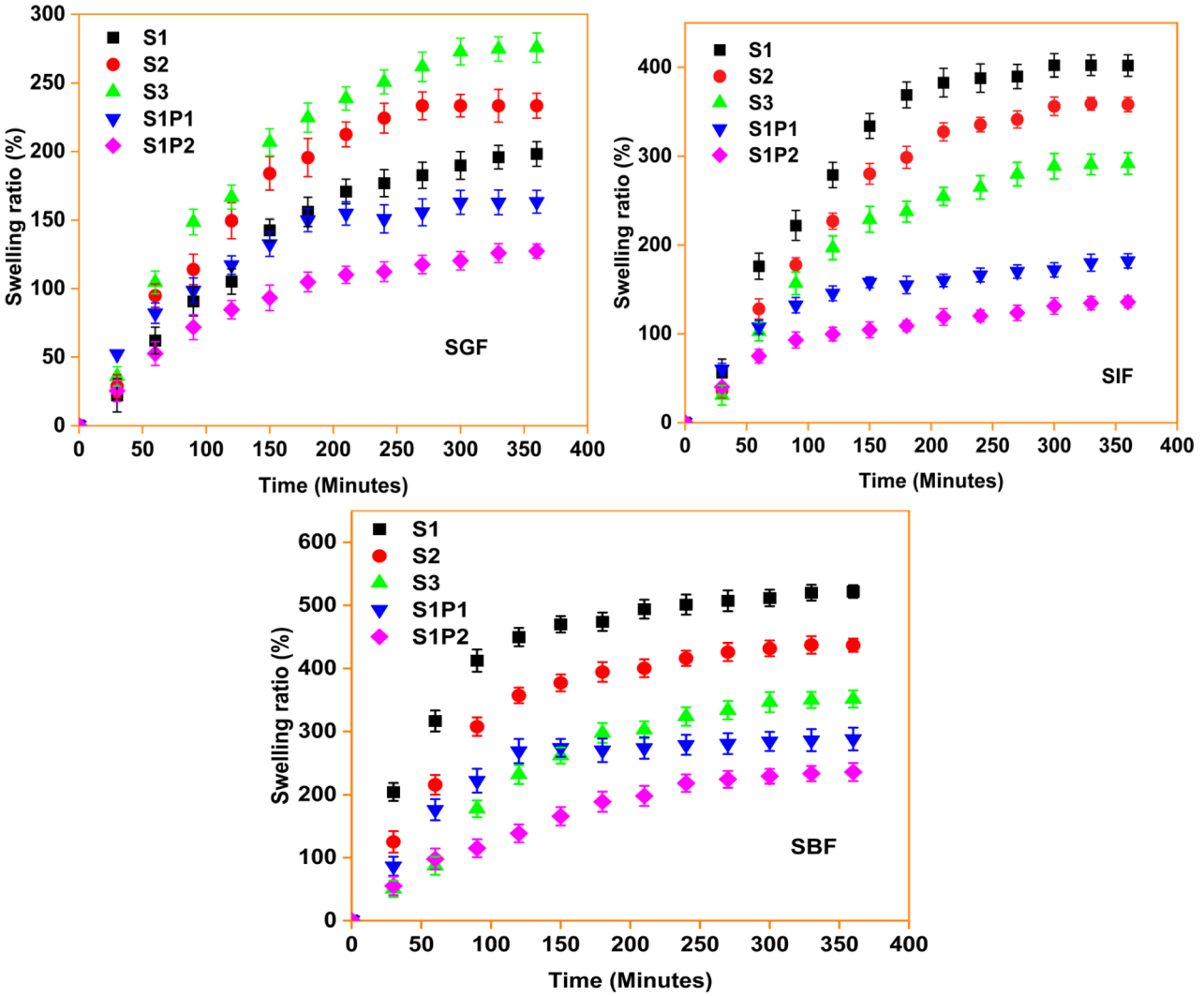

Fig. 9 SR (%) of hydrogels S1, S2, S3, S1P1, and S1P2 in SGF, SIF, SBF.

hydrogels. The SR (%) of the hydrogels, in SBF is generally higher than in SIF and SGF, which is attributed to deprotonation of –COOH groups of SA in alkaline medium (pH 7.4). Consequently, the electrostatic repulsions between carboxylate groups (COO^-) cause polymer relaxation and the diffusion of the fluids into the hydrogels. The obtained SR (%) demonstrates, as the $CaCl_2$ content rises from 1% to 5%, crosslinking density increases, hydrogels become more compact and stiff, and the extent of swelling reduces. As seen in the graph, the swelling behavior of the hydrogel S1P1 ($CaCl_2$, 1%) is unstable, which may be due to insufficient polymer crosslinking.

The SA/PVP hydrogels displayed lower swelling ratio (SR%) in simulated gastric fluid (SGF, pH 1.2) due to the stability of sodium alginate (SA) in the gastric medium. These exceptional characteristics of the SA/PVP hydrogel protect TNZ from the harsh gastric conditions and prevent immediate drug release in the stomach, allowing the drug to reach the intestines and colon at an optimal therapeutic dosage. Considering the lowest SR% in SGF and the optimal SR% in simulated body fluid (SBF), the SA/PVP hydrogel with a 3 : 1 weight composition, crosslinked with 3% $CaCl_2$, was chosen as the most suitable hydrogel composition for TNZ *in situ* loading. This specific composition ensures effective drug delivery by balancing stability in the gastric environment and optimal swelling in the intestinal environment.

3.8. Porosity measurement

One of the most important physical characteristics of hydrogels for their use as CDRSs is their porosity which influences the degree of swelling and rate of drug release. Fig. 10, shows the change in the percent of porosity of the SA/PVP hydrogels with respect to the polymer proportion and concentration of crosslinking agent. The result shows that an increase in porosity is obtained with an increasing amount of PVP. The hydrogel S3 showed the highest porosity (91.95 ± 1.01%) while the lowest porosity of about 74.61 ± 1.33% was obtained for the hydrogel S1. The formation of a more significant number of crosslinked channels comprised of void spaces formed during the interweaving of PVP ring chains into the SA networks, causing the steady increase in porosity with increasing PVP amount.[40]

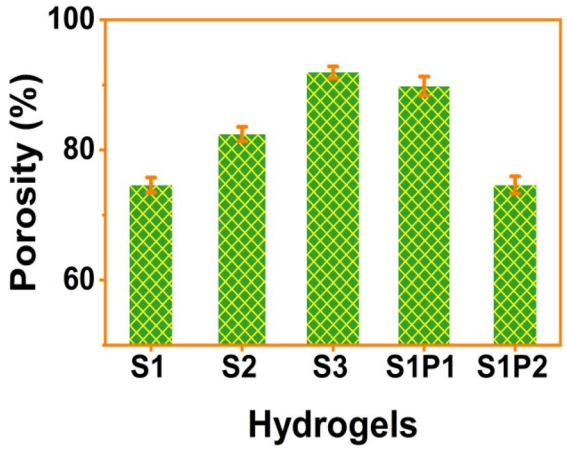

Fig. 10 Porosity of the hydrogels.

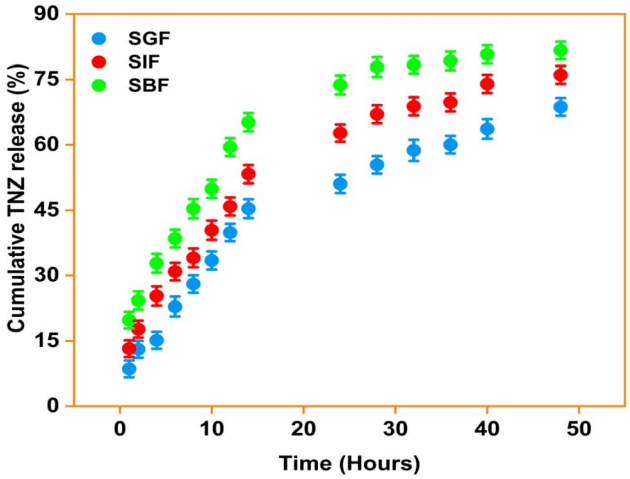

Fig. 11 *In vitro* cumulative TNZ release from the hydrogel TNZ–S1 at 37.2 °C.

Further, the decreased porosity with increasing SA content is due to the ionotropic crosslinking of SA chains through $CaCl_2$, resulting in compacted network structure. It is observed that porosity decreased steadily as a function of the concentration of $CaCl_2$. The hydrogel S1P1 with 1% $CaCl_2$ showed the highest porosity of about 89.82 ± 1.46%, whereas the hydrogel S1P2 with 5% $CaCl_2$ had the lowest porosity of approximately 66.45 ± 1.32%. This shows that, as the concentration of $CaCl_2$ increases, so does the crosslinking density, resulting in the formation of stronger and denser hydrogel structures. In this study the hydrogel S1 having porosity of approximately 82.93 ± 1.1% is selected as an effective hydrogel composition for the colon specific controlled release of TNZ.

3.9. Drug release profile

The *in vitro* release of the drug from crosslinked hydrogels is influenced by the porosity and swelling properties of the hydrogels.[41] As shown in Fig. 11, the cumulative drug release of TNZ was investigated *in vitro* in simulated fluids of various pH (1.2, 6.5, and 7.4). The release profile shows increasing trend as a function of time, regardless of changes in the pH of the releasing medium. The amount of TNZ released (%) from the hydrogel in SGF, SIF, and SBF is approximately 51.03 ± 2.06%, 66.68 ± 1.98%, and 73.74 ± 2.19% at 24 hours, respectively.

The highest cumulative release of TNZ (about 81%) was obtained in SBF (pH 7.4), and the lowest cumulative release of TNZ (about 68%) was achieved in SGF (pH 1.2) within 48 hours. In acidic medium (SGF), SA ($pK_a = 3.4$) is get protonated, forming stable algenic acid, which reduces the hydrogel swelling, resulting in relatively a decreased cumulative release of TNZ.

At higher pH (6.5 and 7.4) SA is deprotonated forming more number of carboxylate groups (COO^-). The electrostatic repulsions between the anionic groups cause polymer relaxation and the diffusion of simulated fluids into the hydrogel networks. Consequently, the hydrogel swells, causing relatively higher cumulative release (%) of TNZ. According to the product data (DrugBank ID: DB00911), marketed TNZ tablet formulation is in immediate release form exhibiting rapid dissolution (30–40 minutes) across the gastrointestinal tract. Hence, TNZ bioavailability in the colon is limited. Therefore, the results of this study reveal a slow and sustained release pattern of TNZ from the optimal hydrogel, which is suitable for colon specific CDRSs.

3.10. Drug release mechanisms

To determine the TNZ release mechanism, the TNZ release profile was evaluated by different mathematical models including: zero-order, first-order, Korsmeyer–Peppas, and Higuchi models. Table 2 shows the results of each linear adapted model of the TNZ release data as a function of the pH of the releasing media.

In order to determine the mathematical model fitted best, the model with the highest R^2 values for TNT release in each simulated fluid was chosen. The result (Table 1) shows that the Korsmeyer–Peppas model is the best fitted kinetic model for TNZ release, with highest coefficients of correlation (R^2) values of 0.9756, 0.9896, and 0.9924 in SGF, SIF, and SBF, respectively. The high R^2 values (close to 1) in each simulated fluid indicate that the Korsmeyer–Peppas model provides the best fit for the experimental data on TNZ release across the simulated fluids. This supports the optimization of drug delivery system designs to achieve desired release rates and therapeutic outcomes. The release exponent '*n*' calculated from the Korsmeyer–Peppas equation for each medium was 0.565 (SGF), 0.642 (SIF), and 0.706 (SBF). The '*n*' values are between 0.43 and 0.89, suggest that the drug release follows time-dependent anomalous (non-Fickian) diffusion. This means that the release process involves a combination of factors, such as drug diffusion through the hydrogel matrix and the swelling or erosion of the polymer matrix controlling the release rate, rather than simple diffusion. This behavior is typical of hydrophilic matrix systems, such as SA/PVP hydrogels, where the release mechanism evolves over time as the matrix swells and the drug diffuses out. Additionally, the release exponent increases with pH, rising from 0.565 in SGF to 0.706 in SBF. This trend suggests that the release mechanism is influenced by the pH of

Table 2 Kinetic data of TNZ released from TNZ–S1 in different simulated fluids

Simulated fluid	Zero order model		First order model		Higuchi model		Korsmeyer–Peppas model	
	K_0	R^2	K_1	R^2	K_H	R^2	n	R^2
SGF	0.034	0.786	0.0423	0.6712	0.1432	0.8892	0.565	0.9756
SIF	0.023	0.778	0.0486	0.6843	0.1562	0.8674	0.642	0.9896
SBF	0.025	0.793	0.0426	0.6776	0.1534	0.8452	0.706	0.9924

the environment, possibly due to changes in the swelling behavior of the polymer matrix or other factors like the solubility or ionization of TNZ under varying pH conditions. The release profile indicates that TNZ is released gradually over time, ensuring a sustained therapeutic effect in the colon.[42]

3.11. Antibacterial efficiency test

Fig. 12 shows the antibacterial activity of the drug-loaded hydrogel (TNZ–S1) against *B. fragilis* (ATCC 25285) and *P. aeruginosa* (ATCC 27853).

As summarized in Table 3, the negative control (S1, unloaded hydrogel) exhibited an inhibition zone of 9.5 mm ± 0.56 mm against *B. fragilis*. The observed inhibitory zone of S1 is attributed to the synergistic effect of SA and PVP. During bacterial–hydrogel interactions, the carboxylic group (–COOH) of SA released protons (H^+), resulting in a pH shift in the media. The pH change disrupts the osmotic balance of the bacterial cell leading to break down of cell wall. The anionic carboxylate ions (COO^-) also inhibit cell metabolism by binding to DNA of bacterial species. Simultaneously, the nitrogen-rich imidazole rings of PVP act as electron donors, adhering to the bacterial membrane and compromising its structural integrity. Furthermore, the imidazole end of the highly water-soluble PVP acts as an electron donor due to the presence of a nitrogen atom and attaches to the bacterial cell walls, causing destruction.[43,44]

Pristine TNZ (positive control) exhibited substantial antibacterial activity against *B. fragilis* with an inhibition zone of about 13.5 ± 0.78 mm. The nitro group of TNZ is reduced *via* the electron transport system, resulting in free $-RNO_2^{\bullet}$, which is thought to be contributing to its antibacterial activity. It has been suggested that the toxic $-RNO_2^{\bullet}$ connects covalently to the DNA of the bacteria, triggering DNA damage and cell death under anaerobic conditions.[44,45]

The drug loaded hydrogel (TNZ–S1) inhibited the proliferation of *B. fragilis*, with an inhibitory zone about 21.26 ± 0.92 mm representing a 123% increase in inhibitory area compared to the unloaded 57% increase over the positive control (pristine TNZ) with 13.5 ± 0.78 mm inhibitory zone. As shown in Fig. 12, the inhibitions zones of the hydrogels against *B. fragilis* were homogeneous signifying a uniform circular diffusion of the drug from the hydrogel matrix into the agar medium. Furthermore, it shows that TNZ was successfully incorporated and dispersed within the SA/PVP hydrogel networks during synthesis. Unlike the pristine TNZ, which offers a rapid but burst of activity, the dug loaded hydrogel (TNZ–S1) served as a reservoir. The swelling of the SA/PVP hydrogel network allows a sustained release of the drug (TNZ). As the $-RNO_2$ groups are reduced in the anaerobic environment forming free radicals which, damage the bacterial DNA, the swelling SA/PVP hydrogel ensure constant diffusion of TNZ causing a more thorough elimination of the colony forming units over extended time.

In contrast, both the drug (TNZ) and the drug-loaded hydrogel (TNZ–S1) exhibited no inhibition zone, and *P. aeruginosa* displayed resistance. Because aerobic bacteria flourish exclusively in the presence of oxygen, they fail to offer the necessary conditions for TNZ reduction. Lacking this reduction, TNZ and the hydrogel (PVP) are unable to generate free radicals

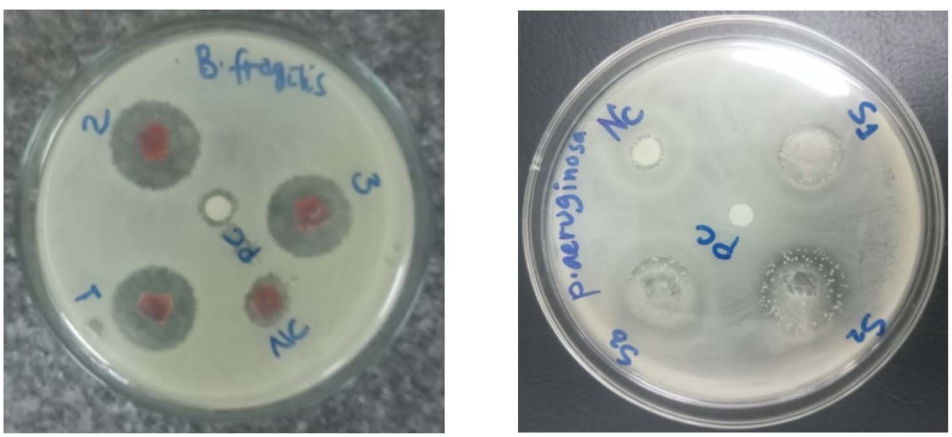

Fig. 12 Disc diffusion tests displaying zone of inhibition shown by TNZ–S1, S1 (negative control), pristine TNZ (positive control) against *B. fragilis* and *P. aeruginosa*.

Table 3 The inhibition zones diameter of hydrogels

	Zone of inhibition, diameter (mm)		
Bacteria strains	S1 (negative control)	Pristine TNZ (positive control)	TNZ–S1
B. fragilis	9.5 mm ± 0.56 mm	13.5 ± 0.78	21.26 ± 0.92 mm
P. aeruginosa	Resistant (R)	Resistant (R)	Resistant (R)

required to inhibit bacterial growth and remain ineffective. Overall, the results show that TNZ–S1 effectively inhibit the growth of the anaerobic bacteria strains, makes it a promising candidate for use in antibacterial applications.

4. Conclusion

The SA/PVP hydrogels displayed lower SR (%) and cumulative drug release in the SGF (pH 1.2) owing to the stability of SA in gastric medium (SGF). These exceptional characteristics of the SA/PVP hydrogel protect TNZ from the gastric harsh conditions and immediate drug release in the stomach, allowing the drug to reach the intestinal and colon at optimal therapeutic dosage. Taking into account the lowest and maximum SR (%) in SGF and SBF, respectively, the SA/PVP hydrogel with a 3 : 1 weight composition, crosslinked with 3% $CaCl_2$, was chosen as the optimum hydrogel composition for TNZ *in situ* loading. As the concentration of $CaCl_2$ increased, the hydrogels exhibited slow biodegradability, amorphous nature, improved thermal stability and mechanical properties owing to increased crosslinking density. In each simulated fluid, drug release followed a progressive increasing trend over time. The highest cumulative release of TNZ (81.6 ± 2.00%) obtained in SCF (pH 7.4) and the lowest cumulative release of TNZ (68.7 ± 2.03%) achieved in SGF (pH 1.2) within 48 hours. The result shows a slow and sustained release pattern of TNZ from the hydrogel, following swelling and diffusion-controlled anomalous mechanism. The enhanced mechanical properties, significant antibacterial activity, and minimal drug release profile in SGF and optimal drug release in SBF; makes the SA/PVP hydrogels promising candidates for colon specific controlled drug release applications.

Conflicts of interest

The authors declare that they have no competing financial interests.

Data availability

The data that support the findings of this study are available from the corresponding author, Zerihun Feyissa Jebessa (PhD), upon reasonable request.

Acknowledgements

The authors are grateful to the experimental support of Adama Science and Technology University, Ethiopia, and SRM Institute of Science and Technology, Kattankulathur, India.

References

1 Z. Han, P. Wang, G. Mao, T. Yin, D. Zhong, B. Yiming, X. Hu, Z. Jia, G. Nian, S. Qu and W. Yang, *ACS Appl. Mater. Interfaces*, 2020, **12**, 12010–12017.
2 H. Patel, R. Singh and B. Datta, *RSC Adv.*, 2025, **15**, 29462–29478.
3 L. Jin, H. Qi, X. Gu, X. Zhang, Y. Zhang, X. Zhang and S. Mao, *AAPS PharmSciTech*, 2020, 1–9.
4 D. Nanda, D. Behera, S. S. Pattnaik and A. K. Behera, *Discover Polym.*, 2025, **2**(1), 6.
5 O. Sreekanth Reddy, M. C. S. Subha, T. Jithendra, C. Madhavi and K. Chowdoji Rao, *J. Pharm. Anal.*, 2021, **11**, 191–199.
6 D. K. Khajuria, R. Vasireddi, M. K. Priydarshi and D. R. Mahapatra, *ACS Omega*, 2020, **5**, 758–765.
7 M. Kurakula and G. S. N. K. Rao, *J. Drug Delivery Sci. Technol.*, 2020, **60**, 102046.
8 F. Oustadi, M. Haghbin Nazarpak, M. Mansouri and F. Ketabat, *Int. J. Polym. Mater. Polym. Biomater.*, 2022, **71**, 14–23.
9 L. Wang, L. Sun, Z. Gu, W. Li, L. Guo, S. Ma, L. Guo, W. Zhang, B. Han and J. Chang, *Bioact. Mater.*, 2022, **15**, 330–342.
10 T. L. Rapp and C. A. DeForest, *Adv. Drug Delivery Rev.*, 2021, **171**, 94–107.
11 C. Rodrigues, C. S. Silva, R. L. Reis, N. M. Neves, P. Lea, A. Oliveira and A. Arau, *Biomacromolecules*, 2022, **23**, 2415–2427.
12 T. Wu, S. Yu, D. Lin, Z. Wu, J. Xu, J. Zhang, Z. Ding, Y. Miao, T. Liu, T. Chen and X. Cai, *ACS Appl. Bio Mater.*, 2020, **3**, 3057–3065.
13 F. F. Magbool, E. Ibrahim Elnima and M. E. Shayoub, *Univers. J. Pharm. Res.*, 2025, **10**, 32–36.
14 D. Nikolova, M. Simeonov, C. Tzachev, A. Apostolov, L. Christov and E. Vassileva, *Polym. Int.*, 2022, **71**, 668–678.
15 A. Shikhani, Y. Atassi, M. Tally and R. Bandakji, *J. Polym. Res.*, 2023, **30**, 1–14.
16 I. Nuran and M. Yi, *J. Ind. Eng. Chem.*, 2017, **52**, 128–137.
17 S. Rajeev, N. H. K. T. and U. G. Panicker, *J. Mater. Chem. B*, 2025, **13**, 12205–12223.
18 P. Hashemzadeh and M. Dinari, *Desalin. Water Treat.*, 2025, **324**, 101520.
19 J. Girón-Hernández, P. Gentile and M. Benlloch-Tinoco, *Carbohydr. Polym.*, 2021, **271**, 12205–12223.
20 P. Date, A. Tanwar, P. Ladage, K. M. Kodam and D. Ottoor, *Chem. Pap.*, 2020, **74**, 1965–1978.
21 W. Deng, Y. Tang, J. Mao, Y. Zhou, T. Chen and X. Zhu, *Int. J. Biol. Macromol.*, 2021, **189**, 890–899.

22 H. Khanum, K. Ullah, G. Murtaza and S. A. Khan, *Int. J. Biol. Macromol.*, 2018, **120**, 1624–1631.
23 H. Khanam, A. Hoque and A. J. Mazumder, *J. Mater. Chem. B*, 2026, 14328–14349.
24 M. Cirri, F. Maestrelli, S. Scuota, V. Bazzucchi and P. Mura, *Int. J. Pharm.*, 2021, **598**, 120375.
25 G. Khan, R. R. Patel, S. K. Yadav, N. Kumar, S. Chaurasia, G. Ajmal, P. K. Mishra and B. Mishra, *RSC Adv.*, 2016, **6**, 100214–100229.
26 A. Kumar, S. Chanda, S. Agarwal, M. Singh, S. Sharma, G. Vasant Bonde and R. Kumar Tiwari, *Mater. Today: Proc.*, 2023, **80**, 1810–1815.
27 A. M. Bakr, A. M. El Nahrawy, A. M. Mansour and A. B. Abou Hammad, *Sci. Rep.*, 2025, **15**, 1–19.
28 R. H. Sizílio, J. G. Galvão, G. G. G. Trindade, L. T. S. Pina, L. N. Andrade, J. K. M. C. Gonsalves, A. A. M. Lira, M. V. Chaud, T. F. R. Alves, M. L. P. M. Arguelho and R. S. Nunes, *Carbohydr. Polym.*, 2018, **190**, 339–345.
29 S. M. Abdellatif Soliman, M. F. Sanad and A. E. Shalan, *RSC Adv.*, 2021, **11**, 11541–11548.
30 P. Ilgin, H. Ozay and O. Ozay, *J. Polym. Res.*, 2020, **27**, 251.
31 N. Naghshineh, K. Tahvildari and M. Nozari, *J. Polym. Environ.*, 2019, **27**, 2819–2830.
32 H. M. Nizam El-Din, D. M. Ibraheim and A. G. M. Rabie, *Int. J. Biol. Macromol.*, 2023, **234**, 123674.
33 L. Zhao, Z. Ren, X. Liu, Q. Ling, Z. Li and H. Gu, *ACS Appl. Mater. Interfaces*, 2021, **13**, 11344–11355.
34 M. Contardi, A. M. M. Ayyoub, M. Summa, D. Kossyvaki, M. Fadda, N. Liessi, A. Armirotti, D. Fragouli, R. Bertorelli and A. Athanassiou, *ACS Appl. Bio Mater.*, 2022, **5**, 2880–2893.
35 A. Dodero, L. Pianella, S. Vicini, M. Alloisio, M. Ottonelli and M. Castellano, *Eur. Polym. J.*, 2019, **118**, 586–594.
36 J. Kurowiak, A. Kaczmarek-Pawelska, A. G. Mackiewicz and R. Bedzinski, *Processes*, 2020, **8**, 304.
37 E. Sharifi, J. Rahbar Shahrouzi, H. Jafarizadeh-Malmiri, S. Ghaffari and A. Baradar Khoshfetrat, *Polym. Bull.*, 2022, **79**, 8883–8903.
38 P. Kowalczyk, P. Trzaskowska, I. Łojszczyk, R. Podgórski and T. Ciach, *Colloids Surf., B*, 2019, **179**, 136–142.
39 M. E. Rabeh, L. K. Vora, J. V Moore, M. F. Bayan, P. Mccoy and M. P. Wylie, *Biomater. Adv.*, 2024, **157**, 213735.
40 S. Ata, A. Rasool, A. Islam, I. Bibi, M. Rizwan, M. K. Azeem, A. ur R. Qureshi and M. Iqbal, *Int. J. Biol. Macromol.*, 2020, **155**, 1236–1244.
41 T. Wu, S. Yu, D. Lin, Z. Wu, J. Xu, J. Zhang, Z. Ding, Y. Miao, T. Liu, T. Chen and X. Cai, *ACS Appl. Bio Mater.*, 2020, **3**, 3057–3065.
42 M. H. Zamani, A. Khatibi, B. Tavana, P. Zahedi and S. Aghamohammadi, *J. Polym. Res.*, 2023, **30**, 1–11.
43 S. U. Khan, M. Sultan, A. Islam, A. Sabir, S. Hafeez, I. Bibi, M. N. Ahmed, S. M. Khan, R. U. Khan and M. Iqbal, *Int. J. Biol. Macromol.*, 2021, **182**, 72–81.
44 M. K. Katual, *World J. Pharm. Res.*, 2017, 809–835.
45 P. Nandy, R. C. Santra, D. Lahiri, M. Nag and S. Das, *ACS Omega*, 2022, **7**, 8268–8280.